Supporting Information

Bio-alcohol Inducing Self-assembly of Heterojunctioned TiO_2/WO_3 Composites into Hierarchical Yolk-shell Structure for Photocatalysis

*Jiehong He†, Pin Lyu†, Dan Li, Can Cheng, Shaoshuai Chang, LianSheng Qin, Chengjin Zhen, Jian Zhu**

Education Ministry Key and International Joint Lab of Resource Chemistry and Shanghai Key Laboratory of Rare Earth Functional Materials, School of Environmental and Geographical Sciences, Shanghai Normal University, Shanghai 200234, China.

† *These authors contributed equally.*

**Corresponding Author: jianzhu@shnu.edu.cn*

Experimental Section

1. Sample preparation

***Synthesis of crystalline TiO_2/WO_3（TWy）composites with hierarchical yolk-shell structure*:** All chemicals were commercially available from Aladdin Co. of analytical grade and directly used without further purification. In a typical procedure, 140.0 μL of $TiCl_4$ (Titanium tetrachloride) was added dropwise into a vigorously mixed solution in a 100 mL round-bottom flask containing 10.0 mL of ethylene glycol and 30.0 mL of tert-butanol. The flask was placed at 40 °C under a flow of argon (20 mL/min) and stirred continually for 1 h. Then, 50.0 mL of 20.0 g/L WCl_6 (Tungsten hexachloride) ethanol solution was added and the solution was stirred for 3 h to achieve a gel. The produced gel was transferred to a Teflon-lined autoclave, aged at 160 °C for 48 h. Then, the product was centrifuged and washed several times with ethanol and water to remove the residual Cl^- and solvent, followed by drying overnight in air at 80 °C. The obtained samples were labeled as TWy. For the further photocatalysis test, the fresh sample was calcined at 550 °C in air for 3 h with heating rate of 2 °C/min and labeled as TWy-550.

Synthesis of TiO_2-550, WO_3-550 and M-TW-550: Pure TiO_2 or WO_3 were also obtained under the same condition of TWy except for using only $TiCl_4$ or WCl_6 as a precursor and labeled as TiO_2-550 and WO_3-550, respectively. M-TW-550 was prepared by a mechanical mixture of TiO_2-550 and WO_3-550 with Ti/W ratio of 1:2.

***Synthesis of C-TWy-550*:** The crushed sample (C-TWy-550) was prepared by grinding the TWy-550 with mortar for 90 mins.

***Synthesis of H-TWy-550*:** 0.1 g of TWy-550 was added to 100 mL of 98 % sulfuric acid under vigorous stirring at 120 °C for 10 h. Then, the product was centrifuged and washed thoroughly with ultrapure water sever times until the solution's pH reached 7, finally dried at 80 °C to obtain H-TWy-550.

***Synthesis of 1.0 wt% Pt-TWy-550*:** Using methanol as sacrificial electron donor, photodeposition method has been performed to prepare Pt-TWy-550. In a typical

synthesis, 100 mg of TWy-550 was dispersed in 80 mL 25 *vol*% methanol aqueous solution containing 0.193 mmol H_2PtCl_6. To completely reduce Pt^{4+} ions, the solution was irradiated for 0.5 h by 300W Xe lamp at 25 °C. The obtained product was filtered, washed thoroughly with ultrapure water several times, then dried at 80 °C for 5 h to obtain 1.0 wt% Pt-TWy-550.

***Synthesis of crystalline TiO_2/V_2O_5 composites with hierarchical yolk-shell structure*:** 140.0 μL of $TiCl_4$ was added dropwise into a vigorously mixed solution containing 10.0 mL of ethylene glycol and 30.0 mL of tert-butanol in a 100 mL round-bottom flask at 40 °C under a flow of argon (20 mL/min). After continuous stirring of above solution for 2 h, 121.0 μL of $VOCl_3$ (Vanadium oxytrichloride) dispersed in 50.0 mL ethanol was added. After another stirring for 1 h, the produced gel was transferred to a Teflon-lined autoclave and aged at 120 °C for 72 h. After then, the product was centrifuged and washed several times with ethanol and water to remove the residual Cl^- and solvent, followed by drying overnight in air at 80 °C.

***Synthesis of crystalline TiO_2/ZrO_2 composites with hierarchical yolk-shell structure*:** 140.0 μL of $TiCl_4$ was added dropwise into a vigorously mixed solution containing 10.0 mL of ethylene glycol and 30.0 mL of tert-butanol in a 100 mL round-bottom flask at 40 °C under a flow of argon (20 mL/min). After continuous stirring of above solution for 2 h, 75 mg of $ZrCl_4$ (Zirconium (IV) chloride) dispersed in 50.0 mL ethanol was added. After another stirring for 1 h, the produced gel was transferred to a Teflon-lined autoclave and aged at 130 °C for 72 h. The product was centrifuged and washed several times with ethanol and water to remove the residual Cl- and solvent, followed by drying overnight in air at 80 °C.

2. Materials characterization

X-ray diffraction (XRD) patterns were recorded on a Bruker D8 Advance X-ray diffractometer with Cu-Kα radiation at a scan rate of 0.02 °/s. The morphologies of the TiO_2/WO_3 samples were measured on a field emission scanning electronic micrograph (FESEM, JEOL JSM-6380LV) and transmission electronic micrograph (TEM, JEM-2010). Energy-dispersive X-ray spectroscopy (EDS) was also performed by the JSM. Diffuse reflection (DR) UV-Vis spectra were obtained on a Shimadzu UV-2450 Spectrophotometer using $BaSO_4$ as a reference. Nitrogen adsorption-desorption isotherms were measured at 77 K with a surface area and pore size analyzer (Quantachrome NOVA 4000e). The surface electronic states were analyzed by X-ray photoelectron spectroscopy (XPS, Perkin-Elmer PHI 5000C). All binding energies were calibrated by using the contaminant carbon (C 1s = 284.6 eV) as a reference. Fourier transform infrared (FTIR) spectra on pellets of the samples mixed with KBr were recorded on a Nicolet Magna 560 FTIR spectrometer at a resolution of 4 cm^{-1}. Photocurrents were measured using an electrochemical analyzer (CHI660D Instruments) in a standard three-electrode system using the prepared samples as working electrodes with an active area of *ca.* 20 × 20 mm^2, Pt as a counter electrode

with the area of 20 × 20 mm^2, and saturated calomel electrode as a reference electrode. A 0.50 M Na_2SO_4 aqueous solution was used as the electrolyte. The bias voltage was 0.50 V (vs. SCE) and a 300 W Xe lamp was used as a light source.

3. Photocatalytic activity

The activity of photocatalytic oxygen evolution was carried out in a sealed irradiation quartz cell (100 mL). In a typically photocatalytic reaction, 50 mg of TiO_2/WO_3 photocatalyst, loaded with 1.0 wt % Pt, was added into 80 mL aqueous $AgNO_3$ solution (0.05 M). The actual amount of Pt was 0.95 wt % measured by ICP. The reaction temperature was maintained at 25°C. Before reaction, the reaction vessel was purged by a mixed flowing gas (CH_4:N_2=1:3) for 5 minutes to completely remove the air. After then, the mixture was sealed and irradiated by four 3 W LED lamps (365 nm) under magnetic stirring. The gas product was analyzed by gas chromatograph equipped with a TCD detector (Shimadzu GC-2014C, 5A molecular sieve column, Ar carrier). Methane was used as the internal standard and the standard curve of oxygen was built under typical reaction condition without any catalysts (R^2 = 0.9999).

Gaseous-phase photocatalytic acetaldehyde degradation was carried out by using a lab-made reactor connected with the gas chromatography. Before the reaction, 50.0 mg catalyst was well dispersed by ultrasonication with anhydrous ethanol in a 55 cm^2 petri dish and dried at 80 °C. Then, the dish loaded with catalyst was placed inside the reactor, and 5.0 uL acetaldehyde aqueous solution ([CH_3CHO] = 1.95 mg/L) was rapidly injected into the reactor. The acetaldehyde gas with a concentration of 993±10 ppm was further pumped for 1 h until reaching absorption-desorption equilibrium. A 300 W Xe-lamp was used as the light source, which was placed at 22 cm away from the bottom of the reactor with the energy density of 115 mW/cm^2. During the reaction, a small portion of reaction gas was collected and analyzed by gas chromatography (Shimadzu GC-2014C) with flame ionization detector. The reproducibility of the results was checked by repeating the experiments at least three times with acceptable limits (±2.5 %).

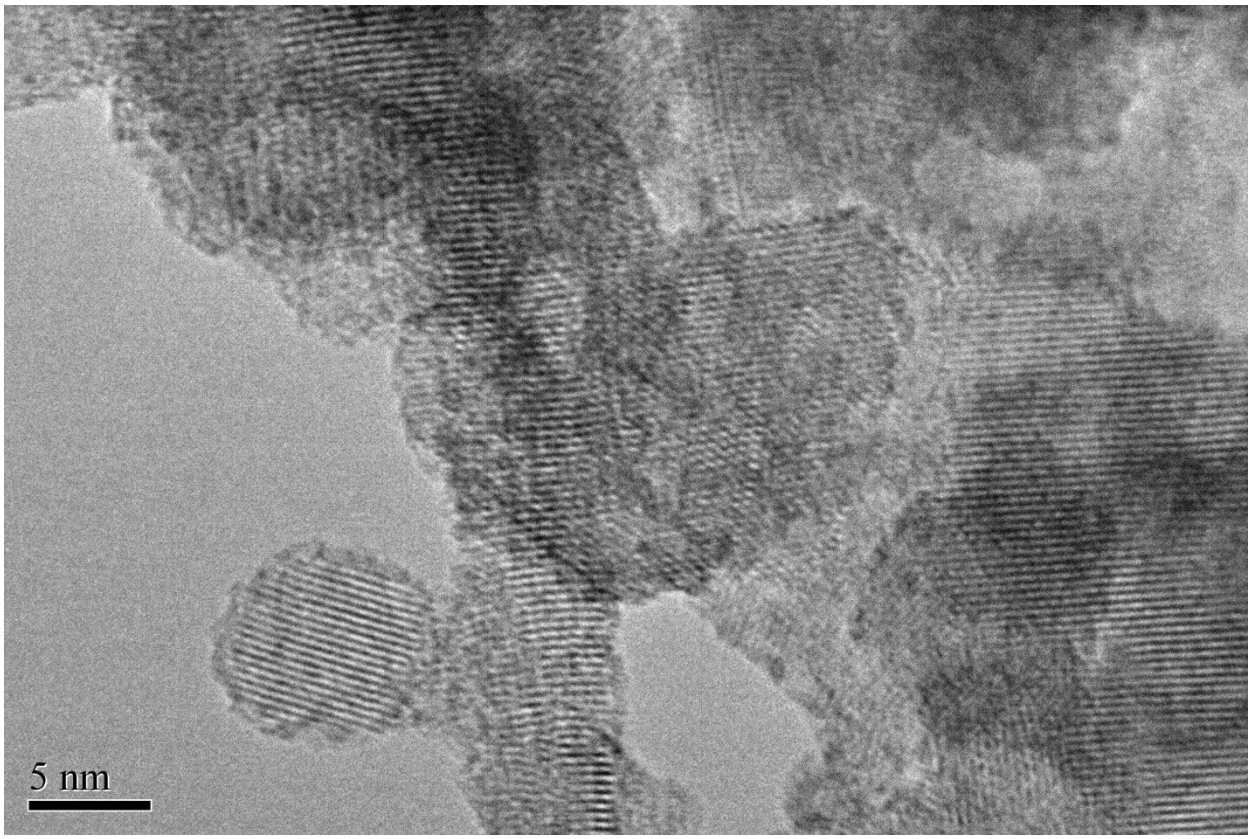

Figure S1. TEM image of TWy-550

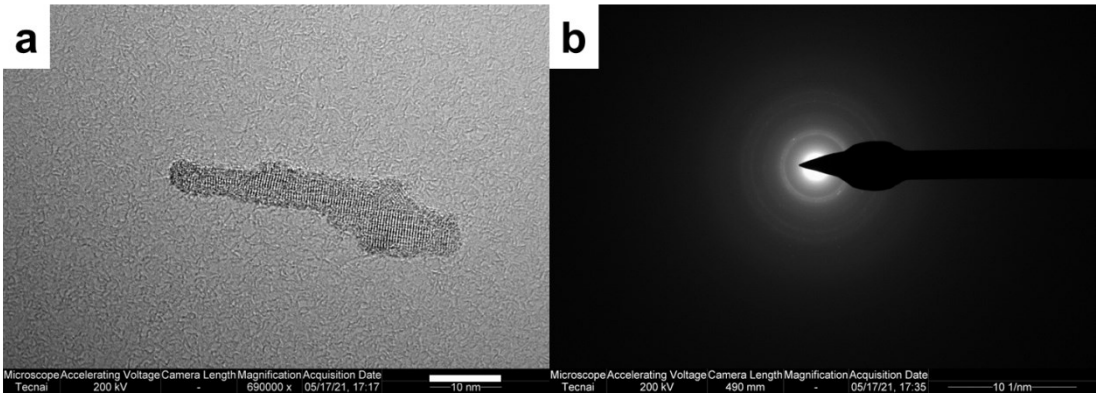

Figure S2. TEM image (a) and SAED pattern (b) of WO_3 nanorod.

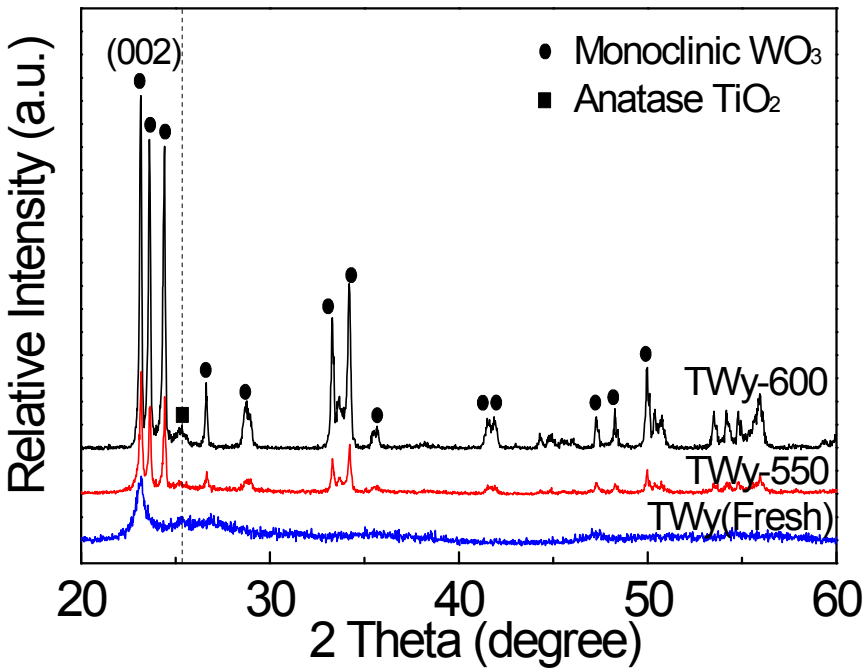

Figure S3. XRD patterns of fresh and calcined TWy samples.

Note: XRD was used to confirms the existence of WO_3 and TiO_2 nanocrystals in TWy. The peaks at 23.1° and 25.3° were consistent with (002) lattice planes of monoclinic WO_3 and (101) lattice planes of anatase TiO_2, respectively. Compared with calcined samples, fresh TWy fails to show all characteristic peaks, possibly due to the relatively low crystallinity and small particle size.

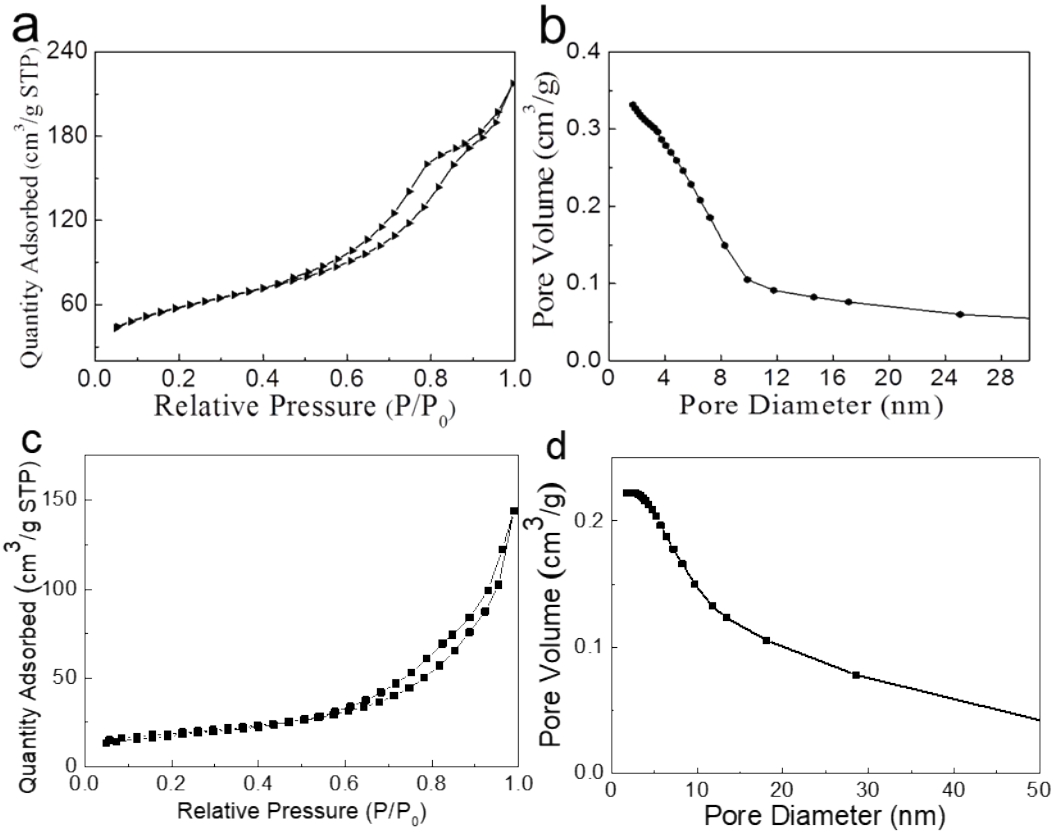

Figure S4. (a) N_2 adsorption-desorption isothermal and (b) pore size distribution of TWy. (c) N_2 adsorption-desorption isothermal and (d) pore size distribution of TWy-550.

Note: The surface area (S_{BET}), pore volume (V_p) and pore size (D_p) were compared between the TWy and TWy-550.

Table S1 The surface area (S_{BET}), pore volume (V_p) and pore size (D_p) of TWy and TWy-550

Sample	S_{BET} (m^2/g)	V_p（cm^3/g）	D_p（nm）
TWy	203	0.45	6.60
TWy-550	64.9	0.22	11.7

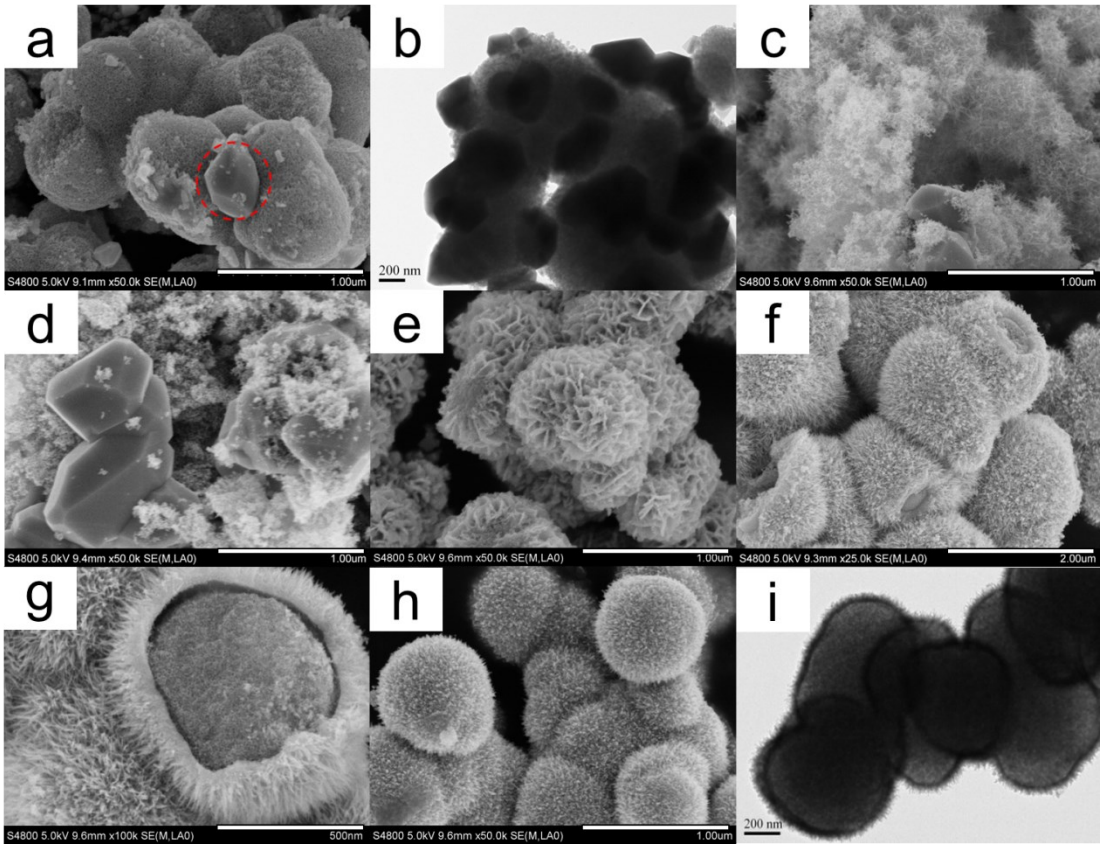

Figure S5. Different morphology of products synthesized under different conditions. (a, b) without using of glycol, (c) adding 2 mL H_2O to glycol, (d) adding 2 mL 1M HCl to glycol, (e) replacing glycol by 1, 3 propylene glycol, (f) replacing glycol by glycerol, (g) replacing glycol by 1, 2 propylene glycol and after reaction for 12 h, (h, i) replacing glycol by 1, 2 propylene glycol. All products except for (g) were obtained after reaction for 48 h.

Note: **Figure S5a and S5b** displayed the morphology of the samples synthesized without using glycol. The bulk monoclinic WO_3 crystals are separated from sphere-like TiO_2 particles (marked by the red circle). Meanwhile, as the formation of yolk-shell structure is sensitive to water, H_2O addition into the glycol solution will also lead to the separation of TiO_2 and WO_3 (**Figure S5c**). Even using HCl to control the hydrolysis rate of Ti^{4+} and W^{6+} precursors, the phase separation of TiO_2 and WO_3 cannot be prevented (**Figure S5d**). Generally, Ti-Cl and W-Cl groups in the precursor are preferential to react with H_2O instead of glycol, which leads to no formation of Ti-R-W BMCs.

In fact, different alcohols produced different Ti-R-W BMCs, which influenced the formation of outer shell and self-assembly rate (**Figure S5e-S5i**). Accompanying the formation of outer shell, carbonaceous species (R) from Ti-R-W BMCs were substituted by hydroxyl groups. Subsequently, these carbonaceous species gradually moved away from the surface of the shell. 1,2-Propylene glycol with larger molecular size than glycol will facilitate the migration of in-situ produced H_2O from the outside solution to the interior space, thus promoting structural evolution from solid to yolk-shell. Glycerol has a similar molecular size as 1,2-propylene glycol but shows an

obvious low self-assembly rate. Another factor to be considered is the much higher viscosity of glycerol (1412 mPa·s, 20 ^{o}C), compared to glycol (22.1 mPa·s, 20 ^{o}C) and 1,2-propylene glycol (60.5 mPa·s, 20 ^{o}C). Such a strong intermolecular force between glycerol molecules greatly retarded mass transfer and slowed down structure evolution.

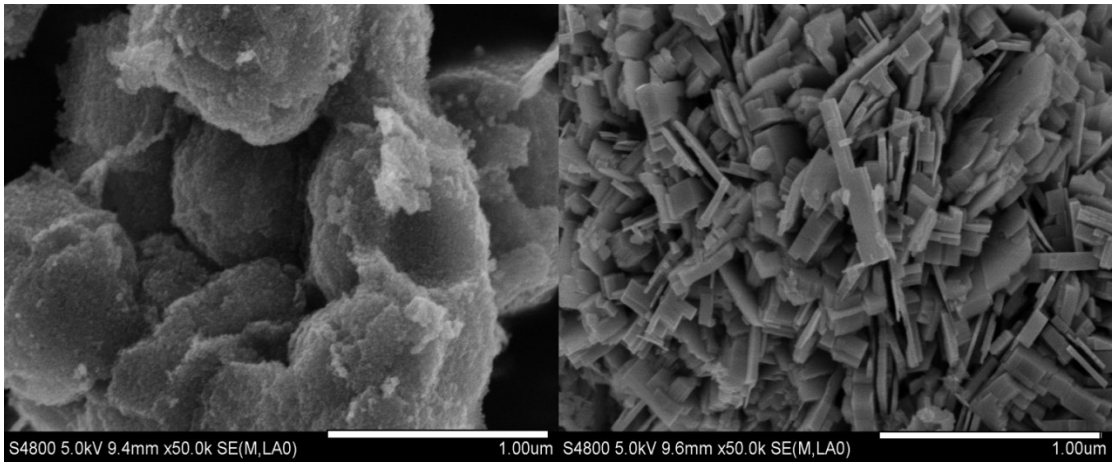

Figure S6. SEM images of fresh TiO_2 and WO_3 samples prepared by using only $TiCl_4$ or WCl_6 as a precursor.

Note: More interestingly, it was found that the position of hydroxyl groups in different alcohols also influenced the morphology of TiO_2/WO_3 composites. When glycol was replaced by 1,3-propylene glycol, the obtained TiO_2/WO_3 composites presented a flower-like structure instead of yolk-shell structure (Figure S5e). The possible reason is that the longer distance between two hydroxyl groups in 1,3-propylene glycol, compared with that in 1,2-propylene glycol or glycol, weakened the hydrogen-bond force between Ti-R-W BMCs, resulting in insufficient strength to form outer shell. Without the outer shell, the in-situ produced H_2O directly migrated into inner cores, followed by continuous self-assembly of sheet-like building block into flower structure. Besides, the molar ratio between $TiCl_4$ and WCl_6 in the precursor was also adjusted to optimize the morphology and structure of TiO_2/WO_3 composites. The optimized ratio between $TiCl_4$ and WCl_6 was 0.5. If this ratio was more than 1.5 or lower than 0.33, the yolk-shell structure disappeared. Meanwhile, using single $TiCl_4$ or WCl_6 as the precursor, only TiO_2 particles or WO_3 nanorods were synthesized, further confirming that the formation of Ti-R-W BMCs was essential for hierarchical yolk-shell structure. Overall, as shown in Scheme 1, the structural evolution initiated from the aggregation of Ti-R-W BMCs into metal-organic spheres, followed by subsequent reaction, dissolution, and re-deposition processes. The in-situ production of H_2O by alcoholysis of Ti^{4+} and W^{6+} precursors facilitated the collapse of inner solid core and formation of hierarchical structured shell.

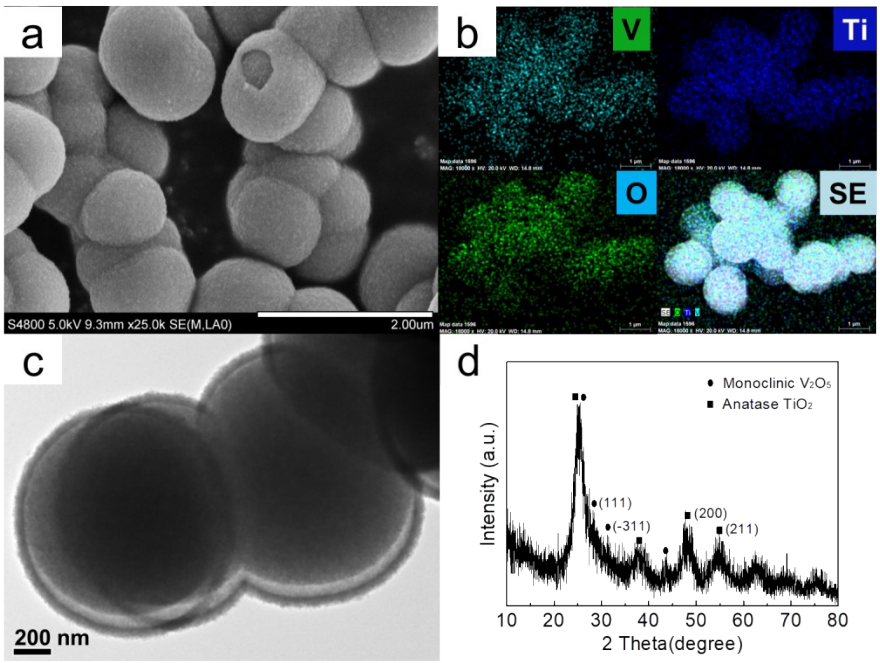

Figure S7. (a) FESEM image, (b) FESEM-EDX elemental mapping, (c) TEM image and (d) XRD pattern of hierarchical yolk-shell structure of TiO_2/V_2O_5 composites.

Note: **Figure S7** showed FESEM and TEM images of TiO_2/V_2O_5 composites, which was similar to TiO_2/WO_3 composite and displayed typical yolk-shell structure with particle size about 1.0 μm. The elemental mapping (**Figure S7b**) demonstrated the uniform distribution of V, Ti and O elements in the composite with no phase separation. The XRD pattern (**Figure S7d**) showed characteristic peaks of both anatase TiO_2 and monoclinic V_2O_5. The peaks at 37.8, 48.0 and 55.0° can be ascribed to (004), (200) and (211) lattice planes of anatase TiO_2 respectively (JCPDS# 21-1272). While the peaks at 28.0, 31.6 and 43.5° was consistent with (111), (-311) and (-510) lattice planes of monoclinic V_2O_5 (JCPDS# 54-0513). The strongest peak at 25.3° was attributed to both (101) lattice plane of anatase TiO_2 and (-111) of monoclinic V_2O_5. The above results demonstrated that the TiO_2 nanocrystals and V_2O_5 nanocrystals were in-situ formed and successfully self-assembled into the yolk-shell structure. Similar results were obtained in the preparation of crystalline TiO_2/ZrO_2 composites with yolk-shell structure (**Figure S8**)

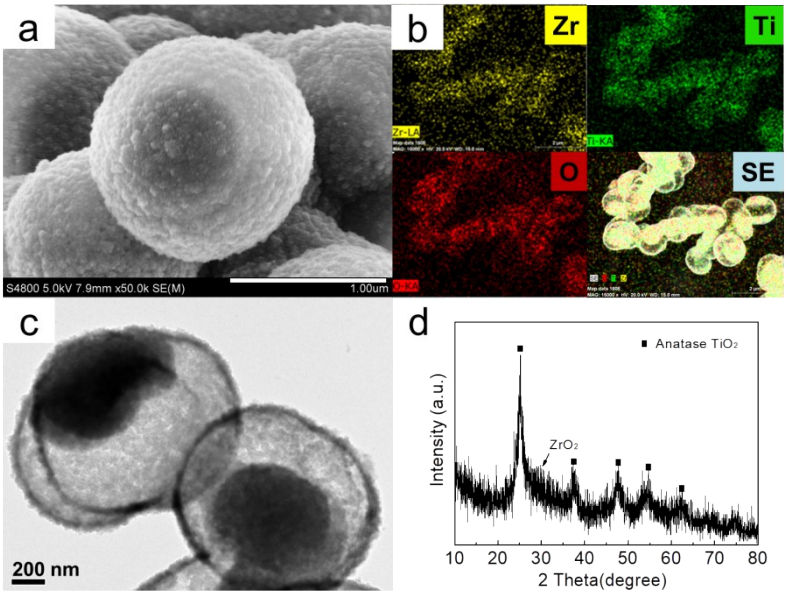

Figure S8. (a) FESEM image, (b) FESEM-EDX elemental mapping, (c) TEM image and (d) XRD pattern of hierarchical yolk-shell structure of TiO_2/ZrO_2 composites.

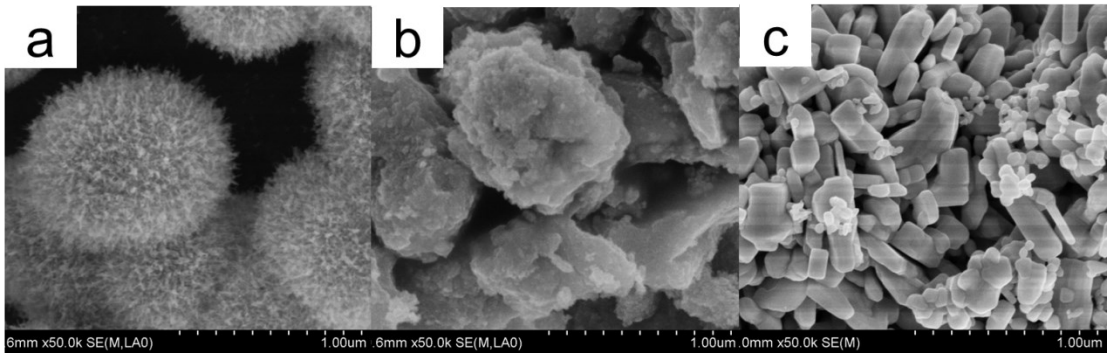

Figure S9. FESEM images of calcined samples (a) TWy-550, (b) TiO_2-550, (c) WO_3-550.

Note: As shown in Figure S9, no obvious morphological change was observed in TWy-550 sample compared to the fresh TWy sample, indicating the high thermal stability of the as-synthesized yolk-shell structure.

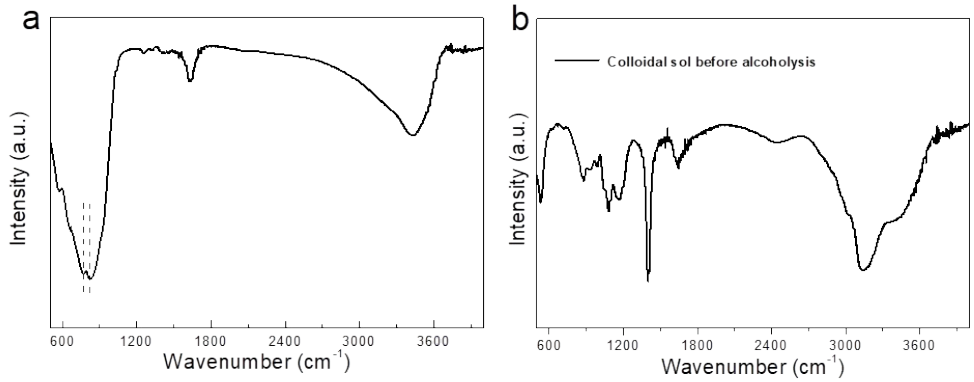

Figure S10. FTIR spectra of (a) TWy and (b) Alcohol mixture with all precursors and Colloidal sol before alcoholysis.

Note: Comparison of TWy (Figure S10) and TWy-550 (Figure 3a), similar result has been observed. No obvious absorption ascribed to organic constituents has been found. So, the wide XRD peaks of TWy are mainly ascribed to the small particle size and low crystallization. The formation of Ti-O-C-C-O-W bridge-linked metal-organic complexes (Ti-R-W BMCs) was confirmed by detailed analysis of Figure S10b. The peak at 1170 cm^{-1} was assigned to the Ti-O-C structure, the peak at 1080 cm^{-1} was ascribed to W-O-C structure and the peak around 3130 cm^{-1} was assigned to C-C structure in colloidal sol before alcoholysis. In this stage, Ti-O-C-C-O-W bridge-linked metal-organic complexes were already formed for further thermal-solvent process. After thermal-solvent process, those peaks disappeared in Figure S10a due to the formation of heterojunctions between TiO_2 and WO_3.

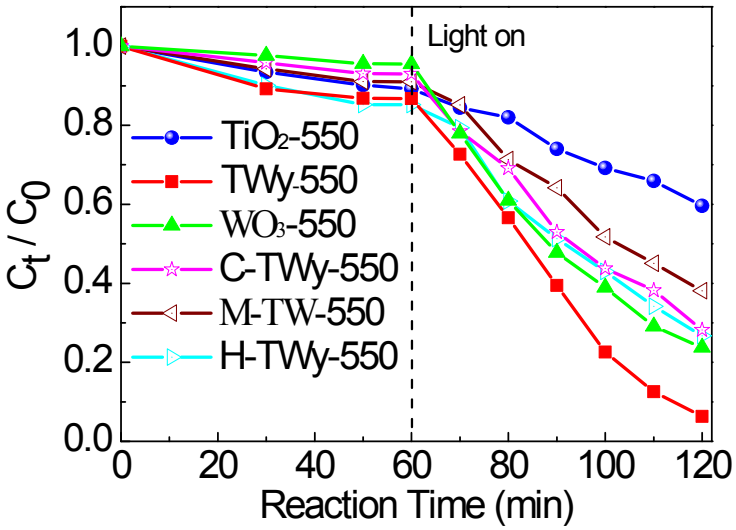

Figure S11. The photocatalytic performance of different samples for acetaldehyde degradation (993±10 ppm) under irradiation of UV-Vis light (300w Xenon lamp, full wavelength).

Note: Mechanical mixture of TiO_2-550 and WO_3-550 with Ti/W ratio of 0.5 (M-TW-550), crushed TWy-550 (C-TWy-550) and TWy-550 etched by H_2SO_4 (H-TWy-550) samples were prepared to demonstrate the superior activity of core-shell structured TWy-550 (Figure 4a and Figure S11). The H-TW-550 sample from mechanical mixture of separate metal oxides would lack intimate contact between two oxides, thus there would be no well-formed interface for the charge transfer resulting in decreased activity. As for the C-TWy-550, the core-shell structure would be destroyed to some extent, which caused the activity to decrease a little bit. By etching with H_2SO_4, the TiO_2 nanoparticles were lost resulting in the low synergistic effect between TiO_2 and WO_3, as well as low activity.

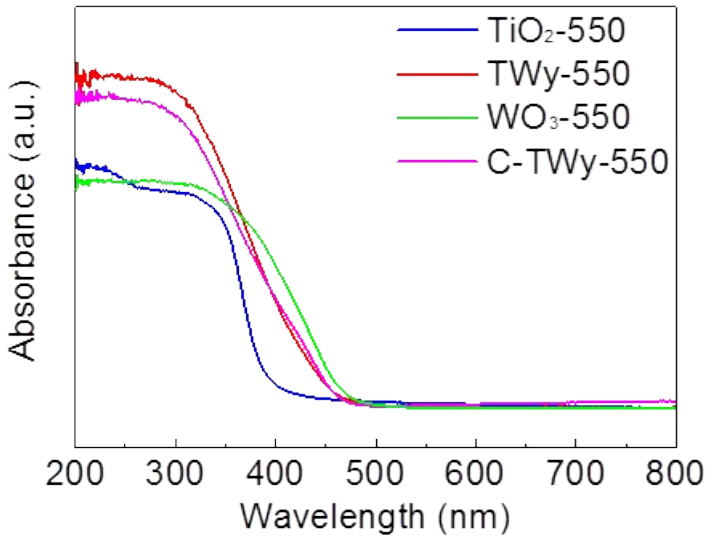

Figure S12. UV-vis diffuse reflectance spectra of TWy-550, TiO_2-550, WO_3-550 and crushed TWy-550 (C-TWy-550).

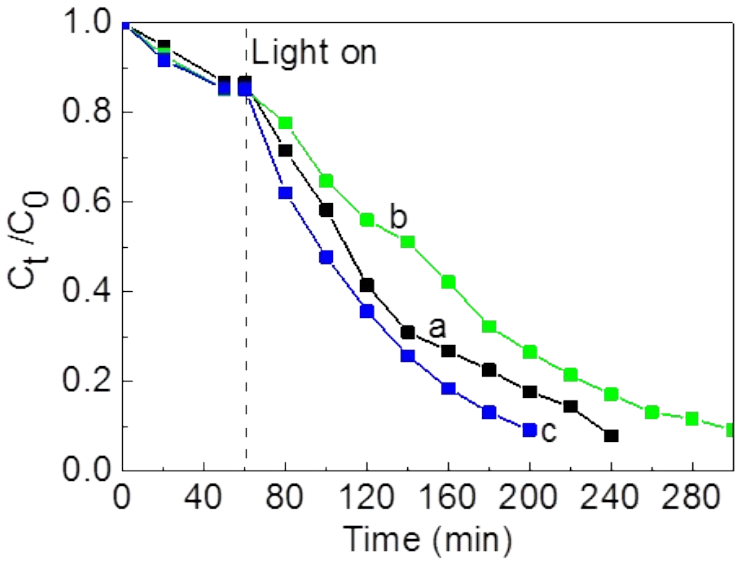

Figure S13. The photocatalytic performance of TWy-550 sample for acetaldehyde degradation (993±10 ppm) under irradiation of (a) UV light (300w Xenon lamp with 365±20 nm filter) and (b) visible light (300w Xenon lamp with >420 nm filter). (c) Photocatalytic activity of Pt-TWy-550 loaded with 1.0 wt % Pt under irradiation of visible light (300w Xenon lamp with >420 nm filter).

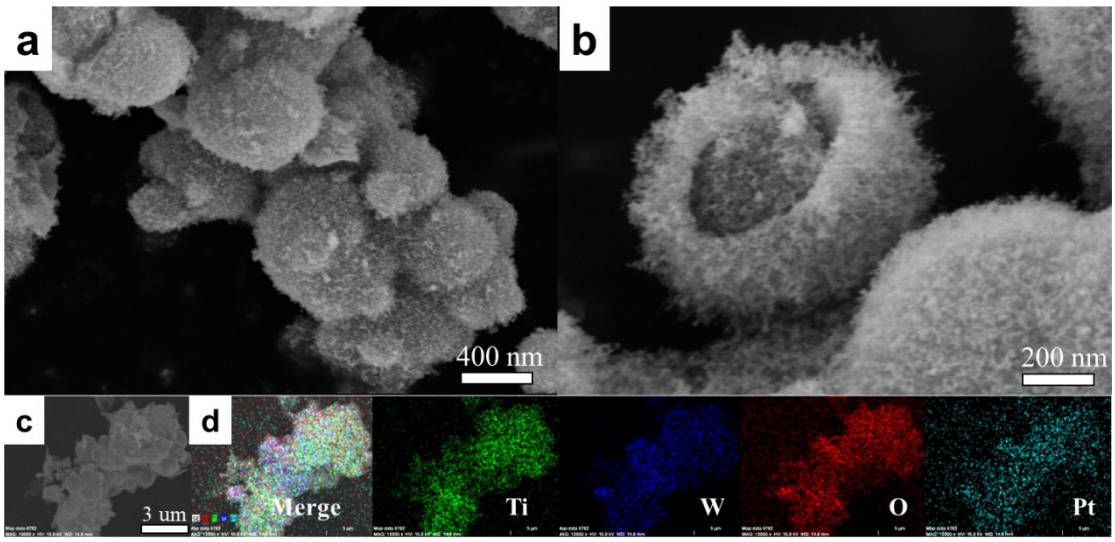

Figure S14. (a, b, c) FESEM image, (d) FESEM-EDX elemental mapping of the Pt-TWy-550.

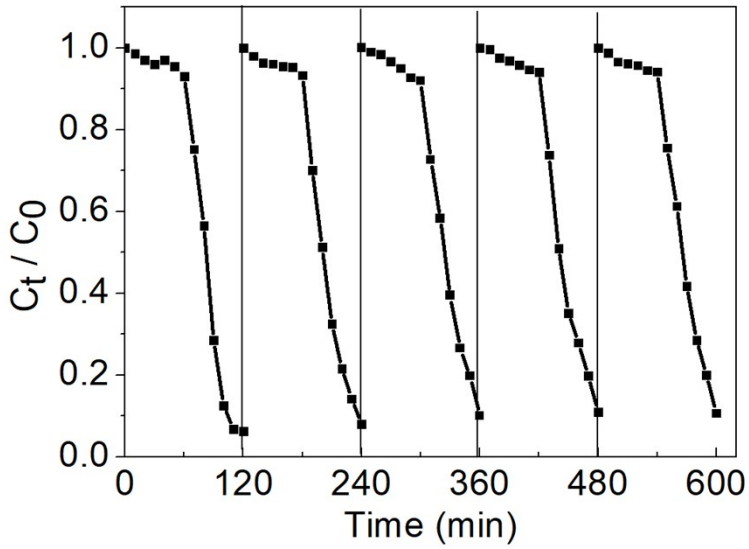

Figure S15. Recyclability of the photocatalytic degradation of acetaldehyde (993±10 ppm) in the presence of TWy-550.

Note: A slight decrease of about 5 % was observed, which may be attributed to the loss of the photocatalysts during the recovery process via centrifugation.